Soft Matter

PAPER

View Article Online
View Journal | View Issue

Cite this: *Soft Matter*, 2015, **11**, 3159

Yielding and flow of highly concentrated, few-layer graphene suspensions

Sebastian Barwich, Jonathan N. Coleman and Matthias E. Möbius*

Received 22nd December 2014
Accepted 2nd March 2015

DOI: 10.1039/c4sm02855d

www.rsc.org/softmatter

For a wide range of applications of graphene suspensions, a thorough understanding of their rheological properties is crucial. We probe the microstructure of dense suspensions of micron-sized, few-layer, defect-free graphene platelets by measuring their viscoelastic properties at various concentrations up to 39 mg ml^{-1}. We propose a model to relate the yield strain to the mesh size of the microstructure as a function of volume fraction ϕ. From the yield stress measurements we infer the typical bond energy ($\approx 20\ k_BT$) and ϕ dependence of the bond number density. These results allow us to express the steady shear viscosity for Peclet number Pe < 10 in terms of the platelet dimensions, bond energy and ϕ using a relaxation ansatz.

1 Introduction

The study of 2-dimensional (2D) materials is currently one of the most dynamic areas of nanoscience. While graphene is probably the most well-known 2D system, many others exist including clays,[1] transition metal dichalcogenides such as MoS_2 and transition metal oxides such as MoO_3.[2] While such systems can usually be grown directly, applications such as conductive ink,[3,4] coatings, composites and energy storage[5] will be facilitated by the ability to produce suspensions of 2D nanosheets in liquids.

Recently, liquid phase exfoliation[6–9] has been developed to produce dispersions of high quality, defect free nanosheets of graphene, MoS_2 and a range of other materials. While such dispersions are ideal for the applications described above, process development will require a thorough understanding of the rheology of these suspensions.

In general, the rheological response of colloidal suspensions beyond the rigidity threshold is dictated by the microstructure of the stress-bearing network that is formed by these particles and the nature of their interaction. In contrast to networks of stiff rods such as carbon nanotubes (CNTs)[10,11] the relationship between microstructure and rheology of suspensions of high aspect ratio graphene platelets beyond the rigidity percolation remains unexplored. In particular it is unknown how yield strain and yield stress scale with the volume fraction ϕ and platelet dimensions. In contrast to graphene oxide (GO) suspensions and clays, whose structure and rheology is sensitive to the surface charges present on these platelets,[12–15] our suspensions of pure, defect-free few-layer graphene platelets provide a well defined model system to study stress bearing networks of high aspect ratio platelets whose interactions are predominantly mediated *via* van der Waals forces.

In this letter we use suspensions of graphene platelets in *N*-methyl-pyrrolidone (NMP) solvent that have been created through liquid exfoliation.[7,8] This process produces suspensions of defect-free, few layer graphene flakes with high aspect ratios of ~1000. The suspension is stabilized against aggregation by the solvent itself as its surface energy is closely matched to that of graphene[8] leading to a vanishingly small enthalpy of mixing.[9] At high concentrations the platelets can bond *via* the van der Waals interaction leading to the creation of a stress bearing microstructure which exhibits a soft glassy rheological response.[14,16] In this work we probe the microstructure of these suspensions by measuring their viscoelastic properties at various concentrations beyond the rigidity percolation.

2 Experimental methods

The graphene suspensions have been prepared *via* liquid exfoliation.[7,8] The solvent is NMP, for which we measure a viscosity of 2.2 ± 0.1 mPa s, which is somewhat larger than the literature value 1.8 mPa s due to water absorption during sample preparation. The exfoliated graphene flakes have typical a length of $D = 1 \pm 0.5$ μm and have on average 3 layers which corresponds to a thickness of $h = 1$ nm (ref. 7) (see inset Fig. 1). The graphene concentrations in our samples range from 1 to 39 mg ml^{-1}, which corresponds to volume fractions ϕ between 4.8×10^{-4} to 0.019. In order to make these highly concentrated suspensions in sufficient quantities, graphite was first exfoliated in NMP using shear exfoliation.[6] The unexfoliated material was removed using coarse filtration with the exfoliated material collected *via* vacuum filtration and then redispersed in fresh NMP using sonication.[7]

School of Physics, CRANN, Trinity College Dublin, Dublin 2, Ireland. E-mail: mobiusm@tcd.ie; Tel: +353-1-896-1055

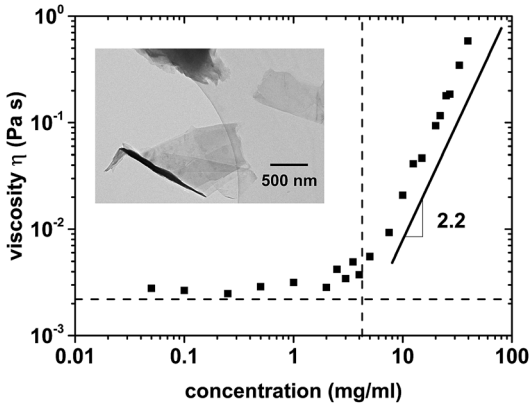

Fig. 1 Viscosity *versus* graphene concentration measured at $\dot{\gamma} = 200$ s^{-1}. The horizontal and vertical dashed lines denote the solvent viscosity ($\eta_s = 2.2$ mPa s) and critical concentration $c_c = 4.2$ mg ml^{-1}, respectively. The black line denotes a logarithmic slope of 2.2. Inset: TEM image of few-layer graphene flakes on a porous grid.

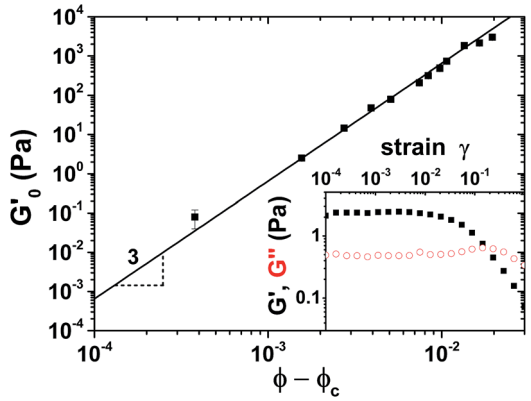

Fig. 2 Storage plateau modulus G_0' *versus* the relative packing fraction $\phi - \phi_c$ measured at 1 Hz. The line is a fit to the data: $G_0' = 0.65(\phi - \phi_c)^3$ GPa. Inset: (■) storage (G') and (○) loss (G') modulus as a function of strain amplitude for $\phi = 0.00356$ (7.5 mg ml^{-1}).

The viscoelastic measurements are performed in a plate–plate geometry using an Anton Paar MCR 301 rheometer. The diameter of the plate and the gap size are 50 mm and 0.5 mm, respectively, allowing oscillation measurements down to shear stresses of 0.1 mPa. The samples were bath-sonicated for 60 minutes prior to loading to ensure a well dispersed suspension. In order to avoid shear alignment we did not prestress the samples. To check that the samples have settled into an equilibrium, we performed consecutive oscillatory strain sweeps which were highly reproducible. The suspensions are stable over experimental time scales. We use the same geometry to measure the viscosity up to strain rates of $\dot{\gamma} = 200$ s^{-1}. For lower concentrations, we use a Couette geometry to measure the viscosities at high shear rates up to 45 000 s^{-1}. The radius of the inner cylinder of the Couette cell is 14.36 mm and it has a gap of 100 μm, which is 2 orders of magnitude larger than the largest platelet dimension.

3 Results

First we determine the critical concentration c_c at which the rigidity percolation occurs. At this point the effective viscosity η of the suspensions increases dramatically and the storage modulus G' becomes non-zero. In order to determine c_c we measured η over a wide range of concentrations at a constant shear rate of 200 s^{-1} as shown in Fig. 1. The viscosity changes little up to 4 mg ml^{-1}, presumably due to shear alignment of the platelets, and then starts to increase dramatically beyond 4 mg ml^{-1} with $\sim c^{2.2}$. A more precise determination of c_c and the corresponding volume fraction ϕ_c comes from measurements of the plateau of the storage modulus, G_0', in the linear response regime. The inset of Fig. 2 shows a typical strain sweep measurement at constant frequency of 1 Hz at a concentration above c_c. In the linear regime, the storage modulus G' exhibits a plateau and is greater than the loss modulus G''. Beyond the yield strain G' decreases and eventually the suspensions is fluidized when $G'' > G'$. This viscoelastic behavior is typical of a soft glassy material. Fig. 2 shows the plateau value of the storage modulus G_0' as a function of the reduced volume fraction $\phi - \phi_c$, where ϕ_c corresponds to the critical volume fraction at which rigidity percolation occurs. Beyond the percolation threshold we expect $G_0' \propto (\phi - \phi_c)^\alpha$, where α is the percolation exponent. We determine ϕ_c by fitting this power law to the data and find $\phi_c = 2 \pm 0.05 \times 10^{-3}$ which corresponds to $c_c = 4.2 \pm 0.1$ mg ml^{-1}.

How does the onset of rigidity ϕ_c depend on the dimensions of platelets? This question has been addressed in the context of conduction percolation[17] and onset of solid-like behaviour in silicate nanocomposites.[18,19] Assuming randomly orientated, monodisperse disc-shaped platelets in solution, one can estimate the percolation threshold as follows.[18] Approximating the flakes as discs with diameter D and thickness h, we embed them in hypothetical spheres of diameter D. Below percolation they are free to rotate within their embedding sphere. As the concentration increases, the randomly dispersed spheres will eventually touch and form a percolating network. At this point, the flakes in the percolating sphere cluster are not free to rotate anymore and a percolating disc network can be formed. The critical overlap concentration ϕ_o is therefore the ratio of the disc volume to the embedding sphere with a prefactor ϕ_j that accounts for the interstices between the spheres: $\phi_o = \phi_j 1.5h/D$.

Ren *et al.*[18] have argued that ϕ_j corresponds to the percolation threshold of (overlapping) spheres ($\phi_j = 0.30$), although the random close pack density, $\phi_j = 0.64$, may be an equally appropriate choice. In both cases, ϕ_o is around 2–4 times lower than the experimentally determined critical concentration $\phi_c = 2 \times 10^{-3}$.

However, this estimate can only be a lower bound. Simulations of (overlapping), monodisperse ellipsoids[20] in the extreme oblate limit ($h/D \approx 1000$), which can be considered a good approximation of discs, have shown that the conduction percolation threshold is somewhat higher, namely $1.27h/D$ while experiments on conductivity percolation of graphite platelets[17] have found critical concentrations in the range $1.3h/D$ to $1.7h/D$. More importantly though, conductivity

percolation is not sufficient for mechanical stability of the network. For mechanical stability of the network, which is necessary for the emergence of a finite yield stress, the platelets require a minimum number of contacts on average. Recent work on jammed packings of frictional ellipsoids have shown that for rigidity the average contact number per particle must be at least 4 in three dimensions.[21] Therefore, one would expect the onset of rigidity at concentrations that are somewhat larger than ϕ_o. Nevertheless, there is agreement in the literature that the critical concentration scales with the inverse aspect ratio h/D. For simplicity we will set $\phi_j = 1$ in the following, *i.e.* $\phi_o = 1.5h/D = 1.5 \times 10^{-3}$, mindful that any small deviations from this value reflect the details of the network structure and are beyond the scope of this study. Such an approach is valid as the exact prefactor in ϕ_o, which is of order 1, is not crucial for modeling the yield strain (eqn (1)).

The percolation exponent α is 3.0 ± 0.1 and close to what is found in graphene oxide composites.[13] In these GO/PMMA composites α is sensitive to the oxide content and goes from 2.4 to 3.1 for decreasing oxide content. Clays, such as Laponite, usually exhibit a lower exponent $\alpha = 2.35$.[15] This result may be compared to simulations of rigidity percolation that incorporate both central and bond bending forces.[22,23] In the absence of bending forces, where bonds only stretch and contract, the percolation exponent is 2.1 ± 0.2, whereas networks in which bonds resist bending as well, this exponent is predicted to be 3.75 ± 0.1. Unlike CNT suspensions for which $\alpha = 2.3 \pm 0.1$ and therefore correspond to central force networks,[10] the exponent for our graphene suspensions is clearly larger and suggests the presence of bending forces. In contrast to the point-like contacts between rods, graphene flakes may form spatially extended contacts that restrict their rotational degrees of freedom. We therefore expect that bond bending forces play a role. However, α is not close to 3.75 either, which suggests that a fraction of bonds is point-like. A platelet may form bonds with its edge or corner, where the latter would correspond to a point-like bond.

We probe the microscopic structure of the graphene network by measuring the non-linear rheological response as shown in the inset of Fig. 2 which shows a typical strain sweep measurement. At low strain amplitudes, the response is linear and mostly elastic ($G' \gg G''$) as indicated by the plateau of the moduli. At larger γ, the suspension becomes fluidized leading to a rapid decay of G'. We define the yield strain γ_c when G' has decreased by a factor of 10. This is illustrated in Fig. 3, where the normalized storage moduli G'/G_0' for different ϕ plotted against γ/γ_c collapse onto a master curve. The inset of Fig. 3 shows the ϕ dependence of γ_c. Higher concentrations give rise to a lower γ_c, a trend that is analogous to CNT's.[10] Close to ϕ_c, the yield strain appears to plateau at around 0.5.

The yield strain depends on the microstructure of the network which in turn depends on ϕ. Below the yield strain, the response is elastic and determined by the bonds stretching and bending and possibly the stiffness of the flakes. At larger strains, the bonds are broken and the response becomes non-linear. For fluidization to occur, the flakes have to rotate through angles large enough to disentangle from the network.

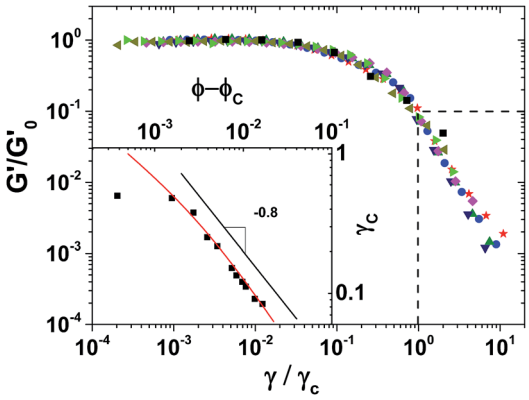

Fig. 3 G'/G_0' *versus* γ/γ_c, where γ_c is shown in the inset. (■) 5, (◀) 7.5, (▶) 10, (◆) 15, (▼) 20, (▲) 22, (●) 25, (★) 33. The dashed lines indicate γ_c where G_0' has decreased by a factor of 10. Inset: γ_c *versus* $(\phi - \phi_c)$. The red line is eqn (1). The black line denotes the logarithmic slope −0.8.

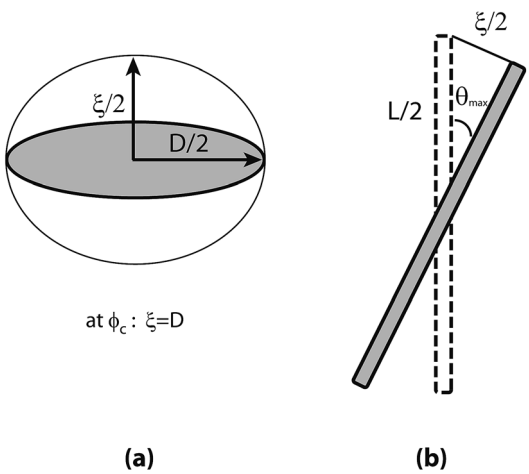

Fig. 4 Estimating the pore size and the yield criterion. (a) Platelet approximated as a disc of radius $D/2$ with thickness h embedded in an ellipsoid to estimate pore size ξ. (b) Illustration of a platelet rotated by θ_{max}.

In order to rationalize the observed scaling of the yield strain with the packing fraction, we employ a model analogous to the one proposed by Hough *et al.* for CNT's.[10]

The flakes will assemble into some disordered network with a typical mesh size ξ. We can establish a relation between ξ and the packing fraction ϕ by embedding the flakes into a packing of oblate ellipsoids with semi-axes $D/2$, $D/2$ and $\xi/2$ as shown in Fig. 4(a). At the rigidity transition, the packing fraction corresponds to flakes being embedded in spheres. Approximating the flakes as discs of diameter D and thickness h, the packing fraction is then simply $\phi = 3h/2\xi$.† At ϕ_c, $\xi = D$ and therefore $\phi_c = 3h/2D = 1.5 \times 10^{-3}$ as determined earlier. Next we estimate the maximum angle of rotation required for fluidization to

† An analogous analysis for rods of diameter D and length L embedded in prolate ellipsoids yields $\phi = 3/2(D\xi)^2$ which is equivalent to a cubic lattice of overlapping rods with lattice constant ξ.[10]

occur. For CNT suspensions it was found previously[10] that the arc length of the maximum angle θ_{max} corresponds to the mesh size ξ assuming an affine deformation and stiff particles. The maximum angle can then be estimated as follows[10] as illustrated in Fig. 4(b):

$$\gamma_c = \tan\theta_{max} \approx \frac{\xi}{\sqrt{D^2-\xi^2}} = \frac{3h}{2D\sqrt{(\phi^2-\phi_c{}^2)}}, \quad (1)$$

since $\xi = 3h/2\phi$, $D = 3h/2\phi_c$.

The agreement between the data and eqn (1) is excellent as shown in the inset of Fig. 3. However, the model predicts a diverging yield strain at $\phi = \phi_c$, which is unphysical as the yield strain should be finite at the rigidity transition of sticky particles. Despite this shortcoming this simple, local model captures the behavior of the yield strain well for ϕ far from ϕ_c.

The model by Shih *et al.*[24] that has recently been used to predict the scaling of G_0' and γ_c in nanoclay composites[25] cannot account for the observed behavior. Far from ϕ_c the model predicts $G' \propto \phi^{(3+x)/(3-d_f)}$ and $\gamma_c \propto \phi^{-(1+x)/(3-d_f)}$, where x and d_f are the fractal dimensions of the elastic backbone and the aggregates, respectively. In our case, where $\gamma_c \propto -0.8$ far from ϕ_c (see inset Fig. 3), that would mean $x = -0.27$ and $d_f = 2.09$. As the fractal dimension should always be positive we conclude the assumptions in that model do not hold here.

Next we look at the shear stress σ measured at 1 Hz as a function of strain amplitude. Fig. 5(a) shows the oscillatory strain sweeps for various ϕ. At low strains, the stress increases linearly up to the yield point at which σ starts to plateau. The yield strain corresponds to rigidity loss due to bond breaking.

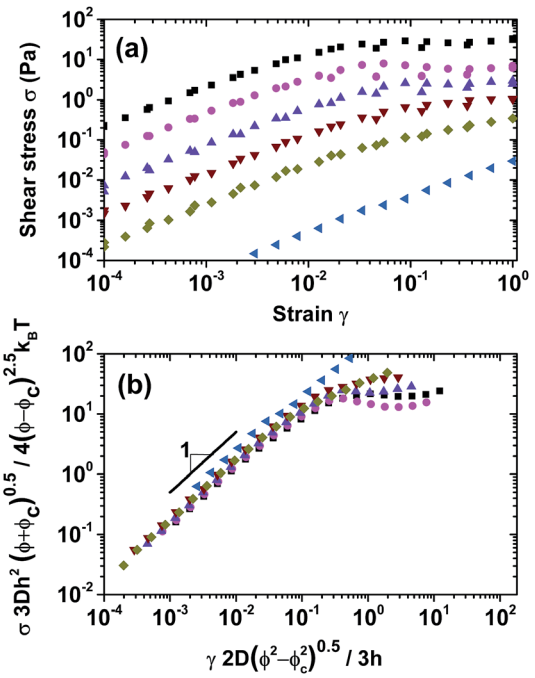

Fig. 5 (a) Shear stress σ from oscillatory strain sweep measurements for different concentrations (in mg ml^{-1}): (◀) 5, (◆) 7.5, (▼) 10, (▲) 15, (●) 25, (■) 39.6. (b) Rescaled stress according to eqn (3) *versus* strain normalized with the yield strain γ_c from eqn (1).

The corresponding yield stress σ_y may therefore be used to estimate the bond energy E_b between the flakes assuming that E_b is ϕ independent. A similar analysis has been done to obtain the interaction energy between CNT's[10] and colloidal spheres.[26] The ϕ dependence of σ_y can be inferred from the elastic response of the material. Up to the yield point the response is elastic, therefore the yield stress scales as $\sigma_y \sim G_0'\gamma_c \propto (\phi-\phi_c)^3(\phi^2-\phi_c{}^2)^{-0.5}$.

The stored elastic energy density at the yield point is $E = 0.5G\gamma_c{}^2 = 0.5\sigma_y\gamma_c$. This may be related to the bond energy E_b assuming that all bonds (or a fixed fraction thereof) are broken at the yield point and that E_b is ϕ independent. Hence, $E = n_bE_b$, where n_b is the bond density. It follows that

$$E_b = \frac{\sigma_y\gamma_c}{2n_b}. \quad (2)$$

For E_b to be ϕ independent, the bond density n_b has to scale as $\sigma_y\gamma_c \propto (\phi-\phi_c)^3/(\phi^2-\phi_c{}^2)$. In order to obtain the prefactor of n_b, it is helpful to express the bond density as the product of the number density n_n and the average number of bonds per particle z. The number density n_n is simply $n_n = \phi/V_g$, where V_g is the volume of the platelet, D^2h. Therefore, the excess bond density (beyond ϕ_c) scales as $(\phi-\phi_c)/D^2h$. It follows that z scales as $(\phi-\phi_c)/(\phi+\phi_c)$ with an unknown prefactor. However, simulations of other disordered jammed systems, such as sphere packings, have shown that this prefactor is of order 1.[27] Substituting eqn (1) and $n_b = (\phi-\phi_c)^2/D^2h(\phi+\phi_c)$ into eqn (2) yields

$$E_b = \sigma_y\frac{3h^2D(\phi+\phi_c)^{0.5}}{4(\phi-\phi_c)^{2.5}}. \quad (3)$$

Interestingly, if ones uses an empirical power law fit for the yield strain (see inset Fig. 3), $\gamma_c \propto (\phi-\phi_c)^{-0.8}$, instead of eqn (1), then $z \propto (\phi-\phi_c)^{0.4}$. The exponent is close to 0.5 found in sphere packings.[21,27] Note that these scalings only hold for large ϕ as one would expect a finite bond density and yield stress/strain at $\phi = \phi_c$.

In order to obtain an estimate for E_b in terms of k_BT we rescale the shear stress, $\sigma 3Dh^2(\phi+\phi_c)^{0.5}/(4k_BT(\phi-\phi_c)^{2.5})$ (eqn (3)), and plot it *versus* the strain normalized by the yield strain (eqn (1)). Fig. 5 shows an excellent collapse of the data onto a master curve. The plateau develops around $\approx 20\ k_BT$. This energy may be compared an estimate of the van der Waals bonding energy between graphene flakes. The surface energy is known[9] to be around $\sim$70 mJ m^{-2}. The interaction energy depends on the geometry of the bond. Bonds across an edge of a flake with area $\sim hD$ have energies of $1.7 \times 10^4\ k_BT$, while a point like contact with area h^2 yields 17 k_BT. The latter value agrees well with the rheology data, we therefore conclude that most bonds are point-like with limited spatial extend, but are not purely central force in nature as indicated by the value of the percolation exponent.

Finally we measure the steady-shear rheology of the graphene suspension for various ϕ above the rigidity transition over a wide range of shear rates $\dot{\gamma}$ as shown in Fig. 6(a). At all ϕ,

the suspensions exhibit shear thinning with a small plateau developing at around $\dot{\gamma} = 10\ s^{-1}$, except for $c = 5$ mg ml^{-1}, where the plateau starts at $\dot{\gamma} = 1\ s^{-1}$. At high shear rates the viscosity approaches the solvent viscosity[28] which is presumably due to shear alignment of the platelets.

Using a relaxation ansatz, we can deduce the steady shear viscosity at low shear rates from the storage modulus and the yield strain. In this approach, steady shear is approximated as a sequence of elastic deformations whose stored energy is dissipated in irreversible microscopic processes on a characteristic relaxation time scale t_r.[29] In our case this would be the bond breaking between flakes at the yield strain. After yielding, the bonds quickly re-form through thermal motion, assuming that the thermal time scale τ is much smaller than the deformation time scale $\dot{\gamma}^{-1}$, *i.e.* Pe $\equiv \dot{\gamma}\tau \ll 1$. For high aspect ratio nanoparticles such as graphene the relevant time scale is the rotational diffusion time scale[30] $\tau = 4\eta_s D^3/3k_BT = 0.7$ s, where we approximate the flakes as disks of diameter D.

The apparent viscosity of the suspension is approximately $\eta \approx G_0' t_r$.[29] Here, t_r is simply the time between consecutive yielding events, thus $t_r = \gamma_c/\dot{\gamma}$. It follows that $\eta \approx G_0'\gamma_c\dot{\gamma}^{-1}$, which reduces to $\eta \approx \sigma_y\dot{\gamma}^{-1}$. Expressing σ_y in terms of the bond energy and platelet dimensions (eqn (3)), we obtain

$$\eta \approx \frac{4E_b(\phi-\phi_c)^{2.5}}{3h^2D(\phi+\phi_c)^{0.5}\dot{\gamma}}. \quad (4)$$

In order to test this relation, we plot the rescaled viscosity $\eta 3Dh^2(\phi+\phi_c)^{0.5}/4E_b(\phi-\phi_c)^{2.5}$ *versus* $\dot{\gamma}$ as shown in Fig. 6(b). For Pe < 10, the rescaled viscosity agrees well with the predicted $\dot{\gamma}^{-1}$ scaling except for $c = 5$ mg ml^{-1} which is close to ϕ_c. Even though this model does not apply for Pe $\gg$ 1, where dissipation is mainly viscous rather than due to bond breaking, the viscosity still scales with $(\phi - \phi_c)^{2.5}/(\phi + \phi_c)^{0.5}$ for $\phi \gg \phi_c$. If one approximates $\gamma_c \propto (\phi - \phi_c)^{-0.8}$ (Fig. 3), then $\eta \propto (\phi - \phi_c)^{2.2}$ as seen in Fig. 1.

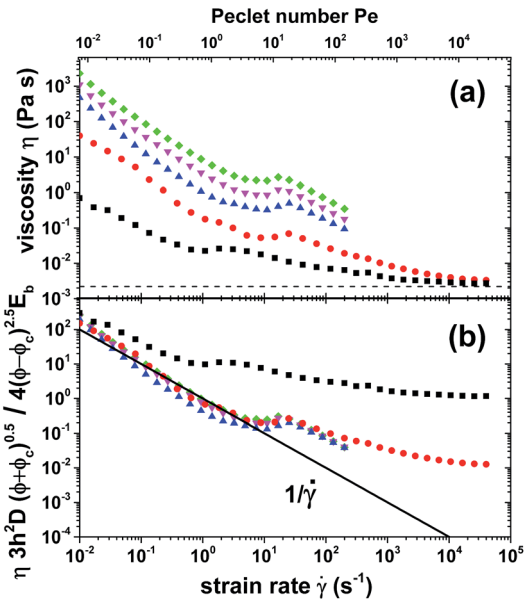

Fig. 6 (a) Apparent viscosity *versus* Peclet number for different concentrations (in mg ml^{-1}): (■) 5, (●) 10, (▲) 20, (▼) 25, (◆) 33. (b) Rescaled viscosity *versus* strain rate $\dot{\gamma}$ for the same data. Here, $E_b = 10\ k_BT$. Black line denotes $\dot{\gamma}^{-1}$ as predicted by the relaxation ansatz.

4 Conclusions

In conclusion, we have probed the microstructure of graphene platelets beyond the rigidity percolation through rheological measurements. The results are consistent with an elastic network of stiff platelets held together by bonds with limited spatial extent of the order of the width of the platelets with an energy of $\approx 20\ k_BT$. The yield strain decreases with concentration due to decreasing mesh size of the network. The steady shear viscosity beyond the rigidity percolation is well described by an relaxation ansatz for Pe < 10 and can be expressed in terms of the platelet dimensions, bonding energy and volume fraction. This result is an important step towards understanding the interplay between microstructure and mechanical response of graphene suspensions.

Acknowledgements

The authors acknowledge support from Science Foundation Ireland under contract numbers G22226/RFP-1/MTR/3135, COST Actions MP1305 and MP1106, PRTLI and Thomas Swan & Co ltd.

References

1 F. Li, K. Lania, X. Wang, G. Xueb and H. Winter, *Soft Matter*, 2010, **6**, 2442–2448.
2 V. Nicolosi, M. Chhowalla, M. G. Kanatzidis, M. S. Strano and J. N. Coleman, *Science*, 2013, **340**, 1420.
3 D. Finn, M. Lotya, G. Cunningham, R. Smith, D. McCloskey, J. Donegan and J. N. Coleman, *J. Mater. Chem. C*, 2014, **2**, 925–932.
4 Q. H. Wang, K. Kalantar-Zadeh, A. Kis, J. N. Coleman and M. S. Strano, *Nat. Nanotechnol.*, 2012, **7**, 699–712.
5 M. Chhowalla, H. S. Shin, G. Eda, L.-J. Li, K. P. Loh and H. Zhang, *Nat. Chem.*, 2013, **5**, 263–275.
6 K. R. Paton, E. Varrla, C. Backes, R. J. Smith, U. Khan, A. ONeill, C. Boland, M. Lotya, O. M. Istrate, P. King, T. Higgins, S. Barwich, P. May, P. Puczkarski, I. Ahmed, *et al.*, *Nat. Mater.*, 2014, **13**, 624–630.
7 U. Khan, H. Porwal, A. ONeill, K. Nawaz, P. May and J. N. Coleman, *Langmuir*, 2011, **27**, 9077–9082.
8 J. N. Coleman, *Acc. Chem. Res.*, 2013, **46**, 14–22.
9 Y. Hernandez, *et al.*, *Nat. Nanotechnol.*, 2008, **3**, 564.
10 L. A. Hough, M. F. Islam, P. A. Janmey and A. G. Yodh, *Phys. Rev. Lett.*, 2004, **93**, 168102.
11 L. A. Hough, M. F. Islam, B. Hammouda, A. G. Yodh and P. A. Heiney, *Nano Lett.*, 2006, **6**, 313–317.
12 D. Li, M. B. Muller, S. Gilje, R. B. Kaner and G. G. Wallace, *Nat. Nanotechnol.*, 2008, **3**, 101–105.

13 H. B. Zhang, W. G. Zheng, Q. Yan, Z. G. Jiang and Z. Z. Yu, *Carbon*, 2012, **50**, 5117–5125.
14 S. Naficy, R. Jalili, S. H. Aboutalebi, R. A. Gorkin III, K. Konstantinov, P. C. Innis, G. M. Spinks, P. Poulin and G. G. Wallace, *Mater. Horiz.*, 2014, **10**, 1039.
15 A. Mourchid, E. Lecolier, H. Van Damme and P. Levitz, *Langmuir*, 1998, **14**, 4718–4723.
16 C. Vallés, R. J. Young, D. J. Lomax and I. A. Kinloch, *J. Mater. Sci.*, 2014, **49**, 6311–6320.
17 A. Celzard, E. McRae, C. Deleuze, M. Dufort, G. Furdin and J. F. Mareche, *Phys. Rev. B: Condens. Matter Mater. Phys.*, 1996, **53**, 6209–6214.
18 J. Ren, A. Silva and R. Krishnamoorti, *Macromolecules*, 2000, **33**, 3739–3746.
19 H. Kim, A. A. Abdala and C. W. Macosko, *Macromolecules*, 2010, **43**, 6515–6530.
20 E. Garboczi, K. A. Snyder, J. F. Douglas and M. F. Thorpe, *Phys. Rev. E: Stat. Phys., Plasmas, Fluids, Relat. Interdiscip. Top.*, 1995, **52**, 819–828.
21 M. van Hecke, *J. Phys.: Condens. Matter*, 2010, **22**, 033101.
22 M. Sahimi, *Applications of Percolation Theory*, CRC Press, 1993.
23 M. Sahimi and S. Arbabi, *Phys. Rev. B: Condens. Matter Mater. Phys.*, 1993, **47**, 703.
24 W. H. Shih, W. Y. Shih, S. I. Kim, J. Liu and I. A. Aksay, *Phys. Rev. A*, 1990, **42**, 4772–4779.
25 J. Vermant, S. Ceccia, M. K. Dolgovskij, P. L. Maffettone and C. W. Macosko, *J. Rheol.*, 2007, **51**, 429450.
26 W. B. Russel, D. A. Saville and W. R. Schowalter, *Colloidal Dispersions*, Cambridge University Press, 1998.
27 C. S. O'Hern, L. E. Silbert, A. J. Liu and S. R. Nagel, *Phys. Rev. E: Stat., Nonlinear, Soft Matter Phys.*, 2003, **68**, 011306.
28 V. Trappe and D. A. Weitz, *Phys. Rev. Lett.*, 2000, **85**, 449–452.
29 T. A. Witten and P. A. Pincus, *Structured fluids*, Oxford University Press, 2004.
30 W. Litchfield and D. G. Baird, *Rheol. Rev.*, 2006, 1–60.

